Chapter 5

The influence of the group environment

So far, I have considered galaxy mergers, interactions, morphology and AGN as causes of quenching across the galaxy population. While it is abundantly clear that these processes can strongly affect the SFHs of galaxies, the density of a galaxy's environment is thought to be the largest influence on the evolutionary path a galaxy will take.

The galaxy environment as a cause of quenching was proposed due to the correlation of environmental density with morphology (Dressler, 1980; Smail et al., 1997; Poggianti et al., 1999; Postman et al., 2005; Bamford et al., 2009), colour (Butcher & Oemler, 1978; Pimbblet et al., 2002) and the quenched galaxy fraction (Kauffmann et al., 2003b; Baldry et al., 2006; Peng et al., 2012; Darvish et al., 2016). Star forming disc galaxies tend to be located in low-density environments with quiescent elliptical galaxies in more dense environments. Although these correlations were originally interpreted as causation, recent evidence from simulations suggests that the environment may not be the dominant quenching mechanism in the galaxy lifecycle (Kimm et al., 2009, 2011; Hirschmann et al., 2014; Wang et al., 2014; Phillips et al., 2015). Perhaps instead, the correlation of increased galaxy quenched fractions with environment is due to a superposition of the effects of mergers, interactions and both mass and morphology quenching.

In order to isolate the cause of the density-morphology and density-SFR correlations, I need to observe how morphology and galaxy quenching timescales change in dense environments with different properties in comparison to the field. Here, I use the group environment to tackle this problem, as this is a more typical environment for a galaxy than the relatively rare rich cluster environment (Carlberg, 2004). I construct a sample of both group and field galaxies and once again use STARPY to determine the quenching time and rate to describe a simple SFH for a galaxy given its photometry. However, dense environments are messy with many possible mechanisms at work, whose effects are difficult to disentangle. The effects of these various mechanisms would be washed out across the population density distributions produced by POPSTARPY and so I do not employ this method in this Chapter.

Instead, I will simplify my analysis in order to separate the effects of the different quenching mechanisms contributing to the galaxy population in the group environment (see Section 5.1.4). I aim to determine the following: (i) How does the environment influence the detailed morphological structures of a galaxy? (ii) Is quenching which is directly caused by the environment occurring in galaxy groups?

5.1 Data and Methods

5.1.1 Group Identification

The construction of a robust cluster or group catalog is a thesis in itself, with many studies attempting this across the SDSS (Merchán & Zandivarez, 2005; Miller et al., 2005; Berlind et al., 2006; Yang et al., 2007; Tago et al., 2008, 2010; Tinker et al., 2011; Muñoz-Cuartas & Müller, 2012; Tempel et al., 2014) and other large surveys (Tucker et al., 2000; Merchán & Zandivarez, 2002; Eke et al., 2004; Cucciati et al., 2010; Robotham et al., 2011; Knobel et al., 2012). The difficulties arise in removing projection effects, understanding the selection function used, covering large ranges in mass and redshift, and dealing with spectral fibre collisions (see comprehensive review by Postman, 2002, for an in depth discussion). Various different methods have been employed to achieve robust group identification including clustering algorithms (e.g. Miller et al., 2005), galaxy colour modelling (Koester et al., 2007), adaptive filter halo modelling (Yang et al., 2005, 2007) and friends-of-friends algorithms (Goto, 2005; Merchán & Zandivarez, 2005; Berlind et al., 2006).

Each group finding algorithm has to be tested for purity (how contaminated the groups are by non-members) and completeness (how often are true members excluded from a group). Campbell et al. (2015) compared the purity and completeness of two of the most frequently used group catalogs of Berlind et al. (2006, a friends-of-friends algorithm) and Yang et al. (2007, a halo modelling algorithm) and concluded that no sample could achieve perfect purity or completeness. Despite the different algorithms employed to identify group galaxies in the two catalogs, Campbell et al. found that the two catalogs are remarkably similar; however the Yang et al. catalog has higher purity of satellites at lower halo masses (i.e. the low halo mass groups are less contaminated by non-members). For this reason the Yang et al. catalog is the most commonly used in environment studies using data from the SDSS (including Hoyle et al., 2011; Pasquali et al., 2012; Wetzel et al., 2014; Shankar et al., 2014; Lacerna et al., 2014; Knobel et al., 2015; Fitzpatrick & Graves, 2015; Lan et al., 2016; Woo et al., 2016; Bluck et al., 2016; Weigel et al., 2016), however I find that when cross matched with the GZ2-GALEX sample (with a $3''$ search radius) only 38 galaxies (of $176,604$ possible galaxies) which belong to a group with 2 or more members are identified. This is most likely due to the necessity for GALEX NUV photometry in this study.

Instead I use the Berlind et al. (2006) catalogue, which when cross matched to the GZ2-GALEX sample and limited to $z < 0.1$ (to ensure GALEX completeness of the red sequence, unlike in Chapter 3; see Wyder et al. 2007; Yesuf et al. 2014) gives $14,199$ group galaxies with the number of group members, $N_{\rm group} \geq 2$. Centrals were selected as the most massive galaxy in a group (as in Yang et al., 2007, 2009; Pasquali et al., 2010) with all other galaxies in a group designated as satellites.

The projected group centric radius, R, of all satellite galaxies was calculated from the projected separations of the co-ordinates of a satellite from its central; this was then converted to kpc from a consideration of the observed redshift of the central galaxy. In order to compare groups of different sizes, the virial radius is used as a normalisation constant to this projected group centric radius. Here I use a proxy to the virial radius, R_{200}(see Navarro et al., 1995), the radius within which the group mass overdensity is 200 times the critical density, $\rho_{\rm crit}(z)$, as defined by Finn et al. 2005:

$$200\rho_{\rm crit}(z) = \frac{M_{cl}}{\frac{4}{3}\pi R_{200}^3}, \tag{5.1}$$

where M_{cl} is the mass of the group. Finn et al. then use the z dependance of the critical density and the virial mass to relate the line-of-sight velocity dispersion, σ_x, to the group mass so that R_{200} becomes:

$$R_{200} = 1.73 \left(\frac{\sigma_x}{1000 \text{km s}^{-1}} \right) \cdot \frac{1}{\sqrt{\Omega_\Lambda + \Omega_o (1+z)^3}} \, h_{100}^{-1} \text{ Mpc}, \tag{5.2}$$

σ_x is calculated for a group as the standard deviation of the velocity dispersions $\sqrt{(v_i - \langle v_i \rangle)^2}$. Here v_i are the proper velocities of each galaxy, i as defined in Danese et al. (1980):

$$v_i = c \cdot \frac{z_i - z_{group}}{1 + z_{group}}, \tag{5.3}$$

where z_{group} is the mean redshift of all the group members. These calculations resulted in a sample of $3,468$ centrals and $10,731$ satellites within a projected group centric radius range of $0.02 < R/R_{200} < 24.9$ and $z < 0.084$ which shall be referred to as the GZ2-BERLIND sample. Note that for a galaxy (central or satellite) to be included in the GZ2-BERLIND sample, the rest of its group does not, however the properties of that group are still retained by the included galaxy.

Unlike in previous Chapters, here I will specifically focus on galaxies that are below the star forming sequence (SFS) in order to simplify the analysis (see Section 5.1.4). I therefore select galaxies that are 1σ below the SFS, giving $4,629$ satellite and $2,314$ central galaxies which will collectively be referred to as the GZ2-GROUP sample. These galaxies are shown in the panels of Figure 5.1 and can be seen to lie below the SFS.

I also compare the GZ2-BERLIND and GZ2-GROUP samples with a measurement of the projected neighbour density from Baldry et al. (2006), $\Sigma_N = N/4\pi d_N^2$, where d_N is the distance to the N^{th} nearest neighbour. Σ is a more direct probe of the local density of a galaxy's environment, and although it does not allow for the identification of groups and their properties, it is still a useful probe of the local density inside a group (see Muldrew et al., 2012, for a comparison of various environment parameterisations).

In this work I use the estimates of Bamford et al. (2009) of a local galaxy density, Σ, determined by averaging $\log \Sigma_N$ for $N = 4$ and $N = 5$. 90% of the GZ2-BERLIND sample have $\log \Sigma > -0.8$ (the threshold quoted by Baldry et al. 2006 below which field galaxies tend to be found), suggesting a completeness of $\sim 90\%$ for the GZ2-BERLIND sample. The distributions of $\log \Sigma$ for star forming and quenching/quenched centrals and satellites in the GZ2-BERLIND sample are shown in Figure 5.2. Star forming galaxies tend to reside in less dense local environments than their quenching/quenched counterparts. The satellite galaxies as a whole also seem to occupy

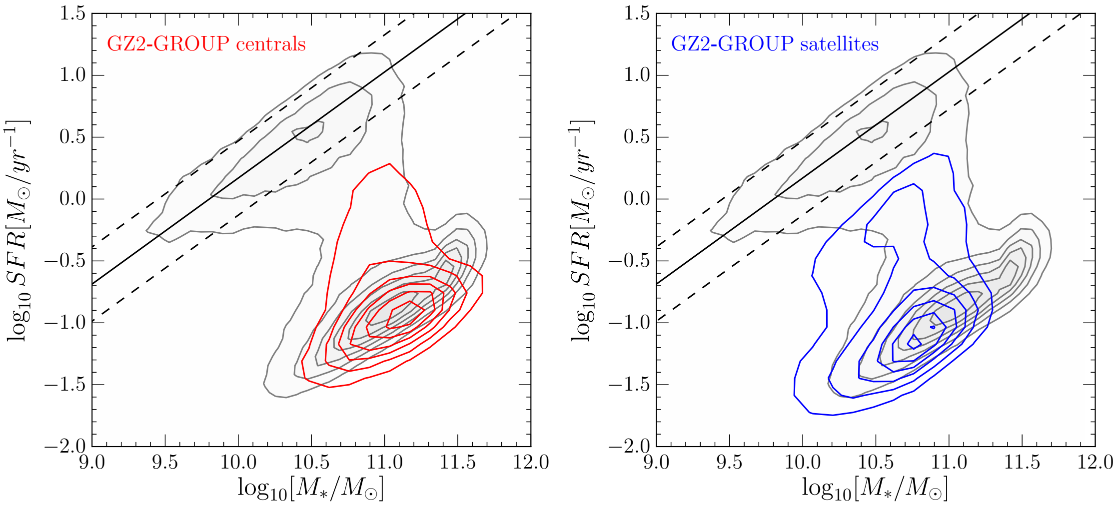

Figure 5.1: The stellar mass-SFR plane showing central (left; red contours) and satellite (right; blue contours) in the GZ2-GROUP sample. In both panels the entire SDSS sample from the MPA-JHU catalog is shown by the grey contours. The definition of the SFMS from Peng et al. (2010) at $\overline{z} = 0.053$ (solid line, the mean redshift of the GZ2-GROUP sample) with $\pm 1\sigma$ (dashed lines) is shown.

denser local environments than centrals, however on investigation this seems to arise because the satellites in the GZ2-BERLIND sample reside in groups with larger N_{group} than the centrals. This is once again likely due to the necessity for GALEX colours. This caveat must be kept in mind as a potential bias to the results presented in Section 5.2.

5.1.2 Field sample

I constructed a sample of field galaxies for use as a control sample to the GZ2-GROUP sample. For all galaxies in the GZ2-GALEX sample, I calculated the smallest projected group centric radii, R/R_{200}, from each of the central galaxies in the Berlind et al. (2006) catalog (regardless of whether the central was included in the GZ2-BERLIND sample) and selected candidate field galaxies as those with (i) $R/R_{200} > 25$ and (ii) $\log \Sigma < -0.8$ (the threshold on the local environment density which selects field galaxies as defined by Baldry et al., 2006). I chose to use both of these environmental density measures to ensure a pure sample of candidate field galaxies.

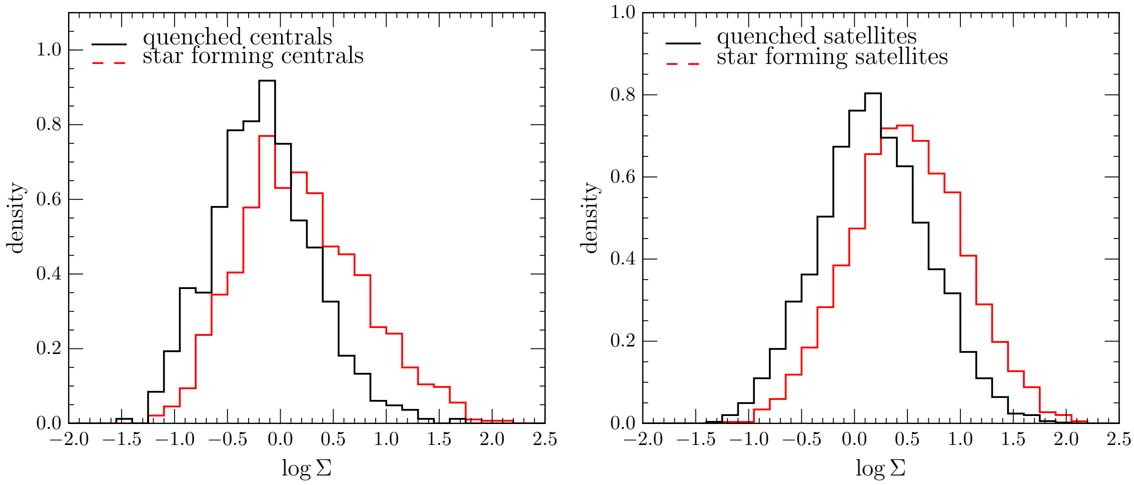

Figure 5.2: Local environment density, $\log \Sigma$, distributions of star forming (black) and quenching/quenched (red) central (left) and satellite (right) galaxies in the GZ2-GROUP sample.

This sample of field galaxy candidates was then matched in redshift and stellar mass firstly to the central galaxies of the GZ2-GROUP sample to give 2,309 field galaxies with $z < 0.084$. In this work I shall focus on galaxies which are either quenching or quenched and are more than 1σ below the SFS and so the same constraints must be placed on this field control sample. This encompasses 1,596 field galaxies with $z < 0.084$ which will be referred to as the GZ2-CENT-FIELD-Q sample. It will be used as a control sample when investigating the trends with central galaxy properties of the inferred quenching parameters. The redshift distribution of the GZ2-CENT-FIELD-Q sample is shown in comparison to the distribution of central galaxies in the GZ2-GROUP sample in left panel of Figure 5.3.

Secondly, the field galaxy candidates were then matched in redshift and stellar mass to the satellite galaxies of the GZ2-GROUP sample to give 5,004 field galaxies with $z < 0.084$ which will be referred to as the GZ2-SAT-FIELD sample. These galaxies in the GZ2-SAT-FIELD sample will be used as a control when investigating the morphological trends of satellite galaxies with environment. Note that the sample is not restricted to being 1σ below the SFS in this case. The redshift distribution of the GZ2-SAT-FIELD sample is shown in comparison to the distribution of satellite galaxies in the GZ-GROUP sample in the right panel of Figure 5.3

We obtain SFRs and stellar velocity dispersions of galaxies for all of the field

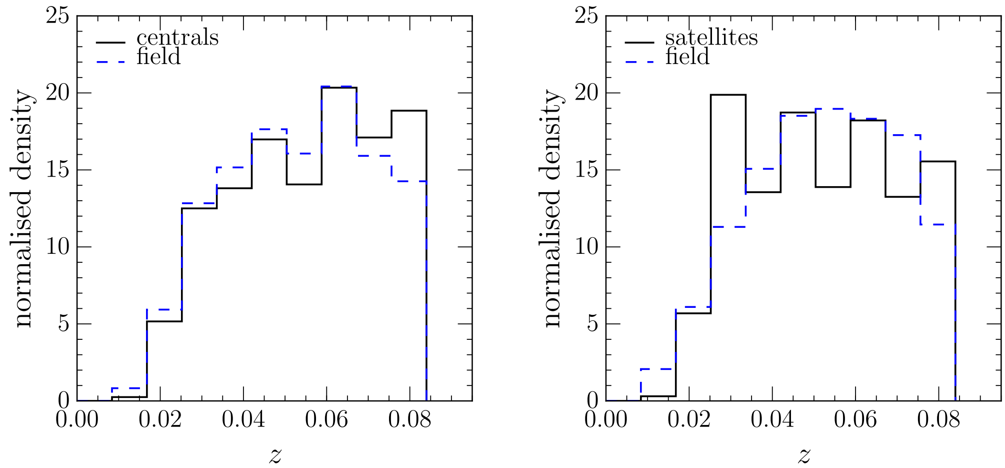

Figure 5.3: Redshift distributions of central (left) and satellite galaxies (right) in the GZ2-GROUP sample (black solid line) in comparison the redshift matched GZ2-CENT-FIELD-Q (left; blue dashed line) and GZ2-SAT-FIELD samples (right; blue dashed line).

samples described above from the MPA-JHU catalogue (Kauffmann et al., 2003b; Brinchmann et al., 2004). Stellar masses were already calculated for the entire GZ2-GALEX sample using the optical photometry and the method outlined in Baldry et al. (2006, see Section 1.1.1).

5.1.3 Morphological fractions

I once again utilise the GZ2 vote fraction to quantity the morphology of galaxies in the GZ2-GROUP sample, in order to investigate the morphological trends with group radius. As in previous Chapters, I shall utilise $p_{\rm disc}$ and $p_{\rm smooth}$ but will also use $p_{\rm bar}$, $p_{\rm bulge}$ and $p_{\rm merger}$ to calculate the bar, bulge and merger fractions in the GZ2-GROUP sample respectively.

Fractions are calculated considering the number of barred (with $p_{\rm bar} > 0.5$; see Masters et al. 2011; Cheung et al. 2013) and bulged (with $p_{\rm bulge} > 0.5$) galaxies over the number of disc galaxies ($p_{\rm disc} > 0.43$, $p_{\rm edge\_on,no} > 0.715$, $N_{\rm edge\_on,no} > 20$; see Table 1.2, originally printed in Willett et al. 2013) in the GZ2-GROUP satellite sample. The merger fraction considers the number of merging galaxies (with $p_{\rm merger} > 0.4$; see Darg et al. 2010b) over the number of galaxies in the GZ2-GROUP satellite sample.

5.1.4 Time since quenching

The SFHs of all galaxies in both the GZ2-GROUP and GZ2-CENT-FIELD-Q samples were analysed using STARPY, the output of which is probabilistic in nature, providing the posterior probability distribution across the two-parameter space for an individual galaxy. Whereas in Chapters 3 & 4 the POPSTARPY method was then used to combine and weight the individual distributions to give an overall distribution representing the population of galaxies, due to the complex nature of the group environment, in this Chapter I instead take the 50th percentile walker position of an individual posterior probability distribution to give the most likely quenching time, t_q and quenching rate, τ, for each galaxy (shown by the solid blue lines in Figure 2.2.2).

This simplifies the output from STARPY for each galaxy from a probability distribution to just two values, with $\pm 1\sigma$ uncertainties (shown by the dashed blue lines in Figure 2.2.2) which encompass the spread of the individual galaxy's SFH posterior probability distribution. In this Chapter I will look for trends in the rate of quenching, τ, and time since quenching onset, Δt, for a given galaxy by calculating $\Delta t = t^{\mathrm{obs}} - t_q$ (where t^{obs} is the age of the Universe at a galaxy's observed redshift; see Section 2.1). I will observe how these quantities change with both group properties, including the halo mass and number of group members, and galaxy properties, including stellar mass, stellar mass ratio, relative velocity of a satellite galaxy and stellar velocity dispersion.

5.2 Results

5.2.1 Mass dependance with radius

Since morphological features have been shown to be dependent on the stellar mass of a galaxy (e.g. the increase in the bar fraction with stellar mass; see Nair & Abraham, 2010; Skibba et al., 2012), before investigating trends in the morphology with group radius in the GZ2-GROUP sample, the mass dependence on the group radius must be considered. This is shown in Figure 5.4. The average mass is roughly flat and consistent with the median field value with increasing group radius, until the most central group radius bin at $R \sim 0.01\ R_{200}$. This trend is present for both morphologies, with early-type galaxies showing a larger increase in the average stellar

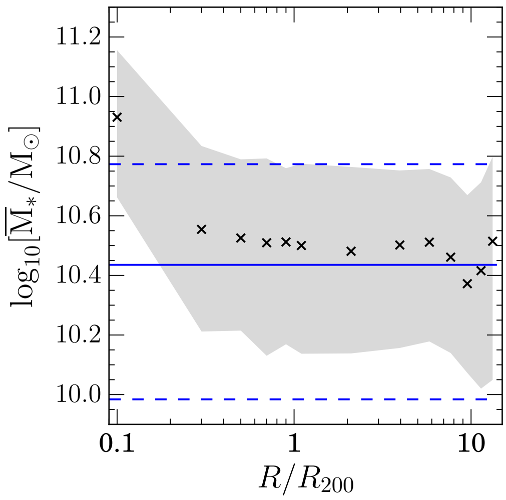

Figure 5.4: The average stellar mass as a function of radius from the group centre. The shaded regions show the $\pm 1\sigma$ in each bin of R/R_{200}. The average stellar mass of the GZ2-SAT-FIELD sample is also shown (blue solid line) with $\pm 1\sigma$ (blue dashed line).

mass. This trend with stellar mass should be kept in mind as a potential bias to the results presented in the following sections.

5.2.2 Dependence of detailed morphological structure with environment

I perform an initial sanity check on the GZ2-GROUP sample by recreating the morphology-density relation of Dressler (1980) in Figure 5.5, which shows the mean disc and smooth vote fractions as a function of group radius. The mean disc vote fraction decreases from the mean field value (blue line) within 1 virial radius, as the mean smooth vote fraction increases, in agreement with previous studies on the morphology-density relation (Dressler, 1980; Smail et al., 1997; Poggianti et al., 1999; Postman et al., 2005; Bamford et al., 2009). The extensive morphological classifications provided by GZ2 also allow for the investigation of how more detailed morphological structure is affected by the group environment.

Figure 5.6 therefore shows how the bar fraction (number of barred disc galaxies over the number of disc galaxies; see Section 5.1.3) increases towards the centre of the group population, significantly over the field fraction (blue solid line). Figure 5.7

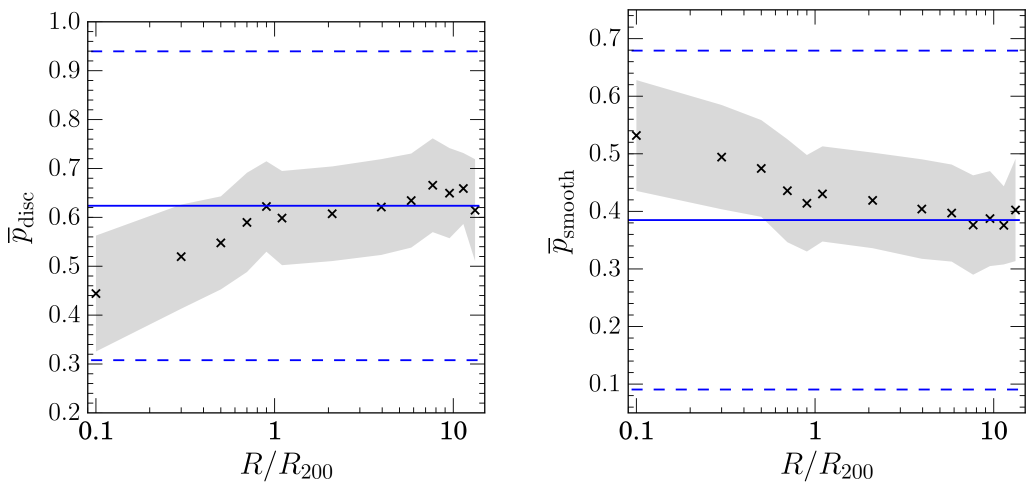

Figure 5.5: Mean GZ vote fraction for disc (top) and smooth (bottom) galaxies in the GZ2-GROUP sample binned in projected group centric radius, normalised by R_{200}, a proxy for the virial radius of a group. The shaded region shows $\pm 1\sigma$ on the mean vote fraction. The mean vote fraction of the GZ2-SAT-FIELD sample are also shown (blue solid lines) with $\pm 1\sigma$ (blue dashed lines).

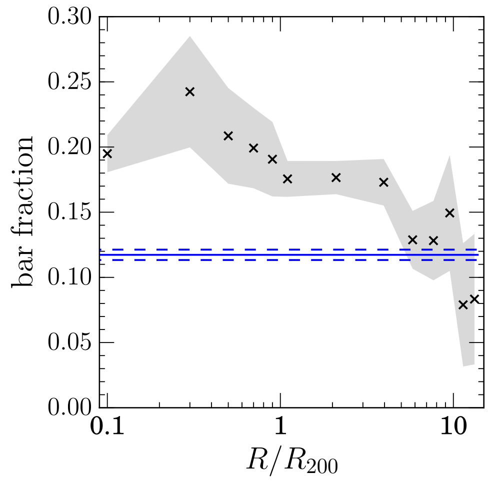

Figure 5.6: Bar fraction (number of barred disc galaxies over number of disc galaxies) in the GZ2-GROUP sample binned in projected group centric radius, normalised by R_{200}, a proxy for the virial radius of a group. The shaded region shows $\pm 1\sigma$ on the bar fraction. The bar fraction of the GZ2-SAT-FIELD sample is also shown (blue solid line) with $\pm 1\sigma$ (blue dashed line).

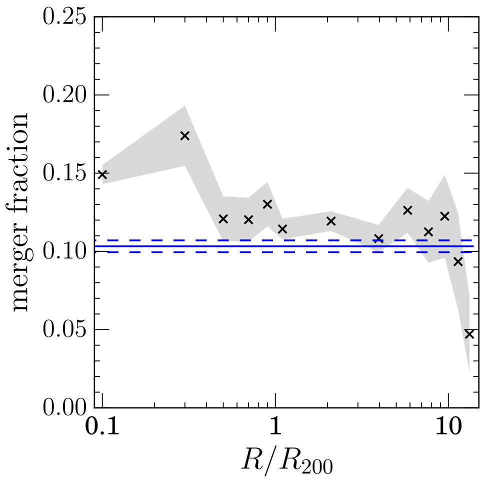

Figure 5.7: Merger fraction in the GZ2-GROUP sample binned in projected group centric radius, normalised by R_{200}, a proxy for the virial radius of a group. The shaded region shows $\pm 1\sigma$ on the merger fraction. The merger fraction of the GZ2-SAT-FIELD sample is also shown (blue solid line) with $\pm 1\sigma$ (blue dashed line).

shows how the merger fraction does not significantly deviate from the field fraction (blue solid line) until within a virial radius. As discussed in Chapter 4, mergers are thought to grow bulges and so similarly, Figure 5.8 shows how the fraction of galaxies with dominant or obvious bulges increases over the field value in the inner regions of the group and the fraction of those with no or just noticeable bulges decreases below the field value within 1 virial radius.

5.2.3 Quenching histories in the group environment

With the output from STARPY I can observe the trends in the time since quenching onset ($\Delta t = t_{obs} - t_q$, see Section 5.1.4) and quenching rate, τ, with group radius, R/R_{200} for satellite galaxies and central galaxies in the GZ2-GROUP sample, compared with galaxies in the GZ2-CENT-FIELD-Q sample. This is shown across Figures 5.9 - 5.11 wherein the GZ2-GROUP sample is binned by various satellite galaxy and group properties. All bin thresholds were chosen to give approximately the same number of galaxies in each bin. Note that this does not ensure the same number of galaxies will be found in each R/R_{200} bin.

Across all the left panels in Figures 5.9 - 5.11 a general trend for increasing time

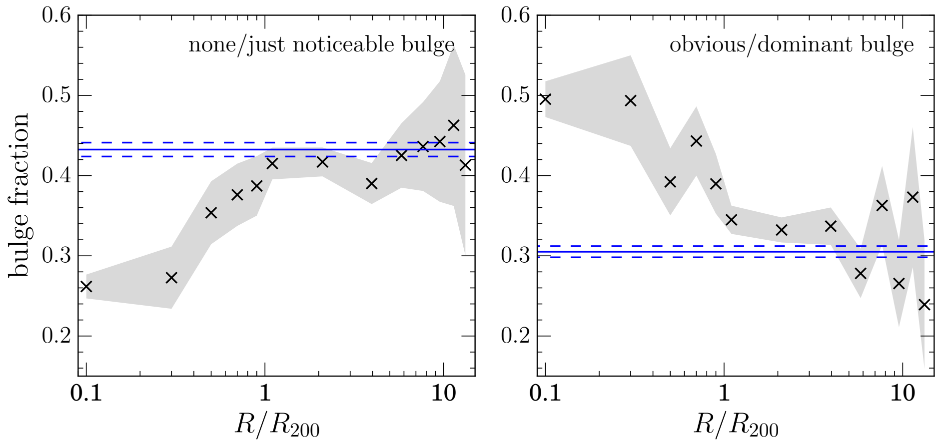

Figure 5.8: Fraction of galaxies with none/just noticeable bulge classifications (left) and with obvious/dominant bulge classifications (right) in the GZ2-GROUP sample binned in projected group centric radius, normalised by R_{200}, a proxy for the virial radius of a group. The shaded regions shows $\pm 1\sigma$ on the bulge fractions. The bulge fractions of the GZ2-SAT-FIELD sample are also shown (blue solid lines) with $\pm 1\sigma$ (blue dashed lines).

since quenching onset, Δt with group radius can be seen. As earlier in Section 5.2.2, in Figures 5.5−5.8 significant differences from the field averages arise under approximately one virial radius. However, no trend with group radius is seen for the rate at which quenching occurs for satellites in the GZ2-GROUP sample (right panels Figures 5.9 - 5.11). This suggests that whatever mechanisms causes quenching in a group will do so at the same rate in both the dense inner and sparse outer regions.

In Figure 5.9a the GZ2-GROUP sample is split by stellar mass, M_*, and a clear trend for increasing time since quenching onset with increasing stellar mass for satellite, central and field galaxies can be seen. However, this trend is less apparent for the rate of quenching seen in Figure 5.9b. The central galaxies (shown by the square points at $\sim 0.01 R/R_{200}$) appear to have quenched more recently than the inner satellites (at $\sim 0.1 R/R_{200}$) of the same mass but have done so at the same quenching rate.

In the bottom panels of Figure 5.9 I split the GZ2-GROUP sample by halo mass by using the stellar mass of the corresponding central galaxy of a group, $M_{c,*}$ as a proxy. I find a clear trend for increasing time since quenching onset with increasing halo mass for satellite, central and field galaxies (Figure 5.9c) but once again this trend is less apparent for the rate of quenching (Figure 5.9d) suggesting the halo mass does

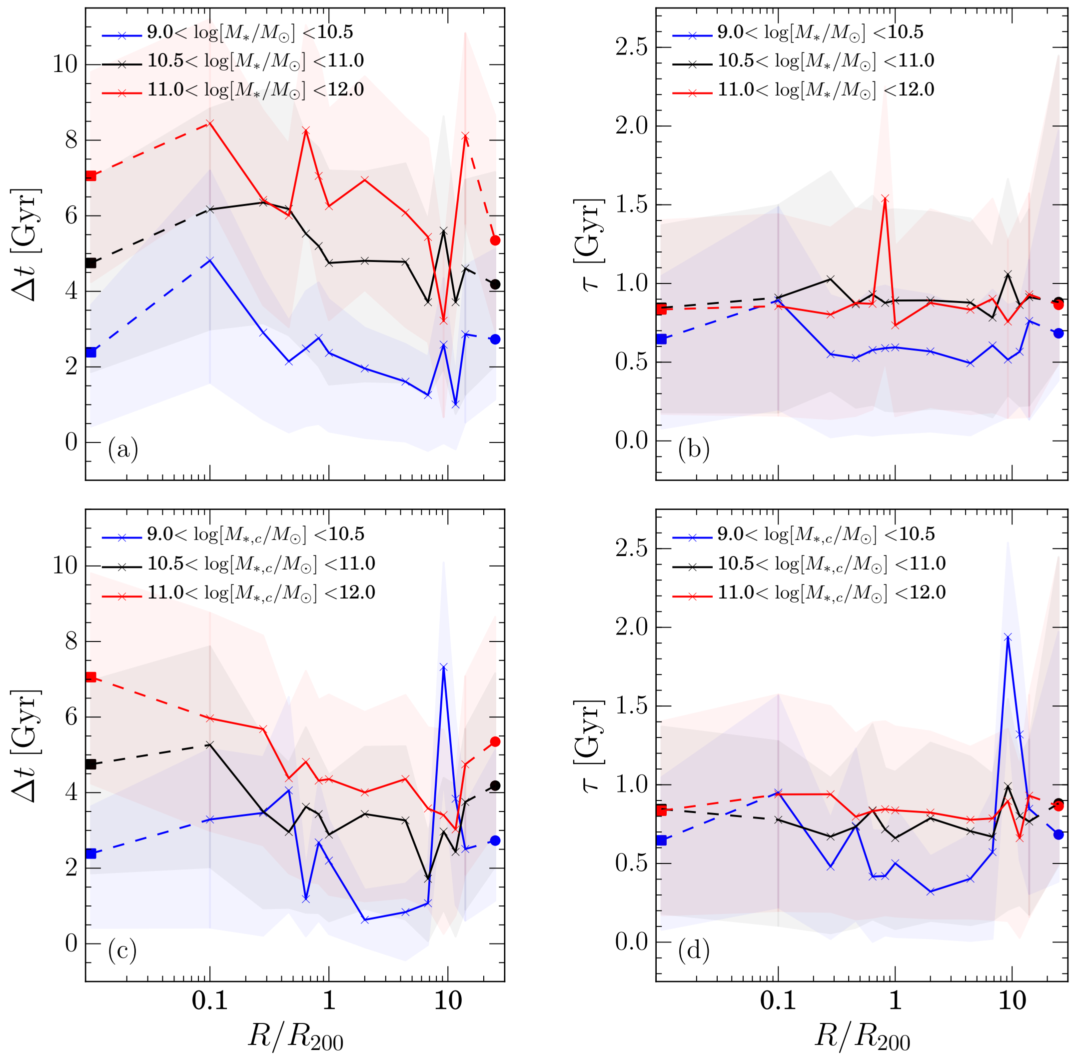

Figure 5.9: The time since quenching onset ($\Delta t = t_{obs} - t_q$; left) and rate of quenching (τ; right) binned in group radius, R/R_{200}, for satellite galaxies (crosses) split into bins of stellar mass (top) and stellar mass of the corresponding central galaxy (bottom; a proxy for halo mass of a group). The corresponding values for central galaxies (squares, plotted at $0.01R/R_{200}$) and galaxies in the GZ2-CENT-FIELD-Q sample (circles, plotted at $25R/R_{200}$) are shown and connected by the dashed lines to help guide the eye. The shaded regions show the $\pm1\sigma$ on Δt and τ in each bin of R/R_{200}.

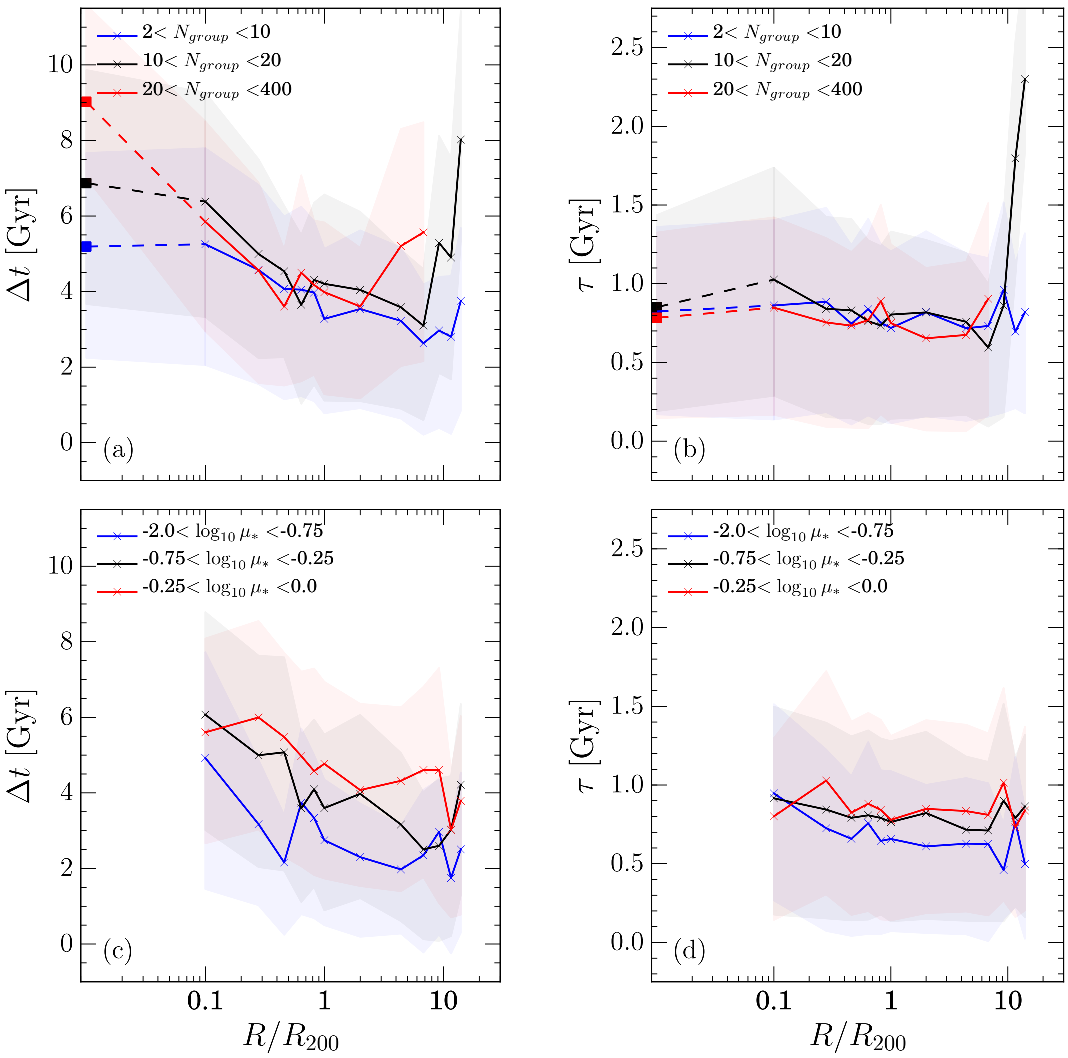

Figure 5.10: The time since quenching onset ($\Delta t = t_{obs} - t_q$) and rate of quenching (τ; right) binned in group radius, R/R_{200}, for satellite galaxies (crosses) split into bins of number of group members (N_{group}, top) and stellar mass ratio ($\mu_* = M_*/M_{*,c}$, bottom). The corresponding values for central galaxies (squares, plotted at $0.01R/R_{200}$) and galaxies in the GZ2-CENT-FIELD-Q sample (circles, plotted at $25R/R_{200}$) are shown, where possible, and connected by the dashed lines to help guide the eye. The shaded regions show the $\pm1\sigma$ on Δt and τ in each bin of R/R_{200}.

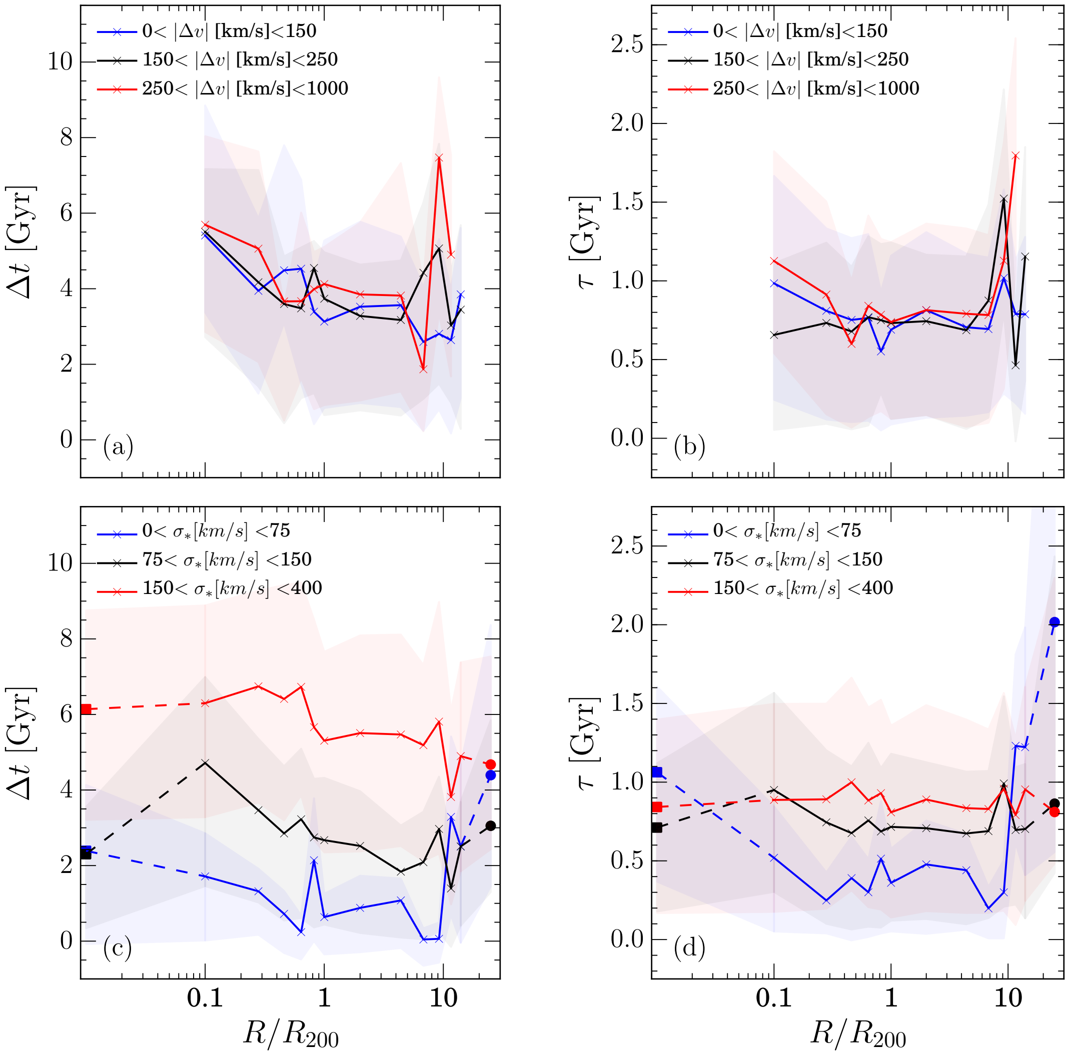

Figure 5.11: The time since quenching onset ($\Delta t = t_{obs} - t_q$; left) and rate of quenching (τ; right) binned in group radius, R/R_{200}, for satellite galaxies (crosses) split by the absolute relative velocity of the satellite to its central galaxy ($|\Delta v|$, top) and stellar velocity dispersion (σ_*, bottom). The corresponding values for central galaxies (squares, plotted at $0.01 R/R_{200}$) and galaxies in the GZ2-CENT-FIELD-Q sample (circles, plotted at $25 R/R_{200}$) are shown, where possible, and connected to the satellite values by the dashed lines to help guide the eye. The shaded regions show the $\pm 1\sigma$ on Δt and τ in each bin of R/R_{200}.

not affect which quenching mechanism acts upon either central or satellite galaxies.

To account for the effects of conformity (Weinmann et al., 2006; Kauffmann et al., 2013; Hearin et al., 2015; Hatfield & Jarvis, 2016, i.e. that satellites of higher mass tend to be found in higher mass halos) I also split the satellites of the GZ2-GROUP sample by the stellar mass ratio of the satellite to its central galaxy, $\mu_* = M_*/M_{*,c}$, in the bottom panels of Figure 5.10. Δt increases more steeply with group radius (particularly within $\sim$ a virial radius; Figure 5.10c) for satellite galaxies with much smaller masses than their group central ($-2.0 < \log_{10} \mu_* < -0.75$, shown by the blue curve). Once again this is not the case for the rate that quenching occurs, as show in Figure 5.10d.

Another property of the group which is expected to affect the satellite quenching histories is the number of group members, N_{group}, which should be roughly correlated with a satellite's local density in a group. The top panels of Figure 5.10 show that there is no trend with time since quenching onset or rate of quenching with increasing N_{group} for satellite galaxies. The central galaxies (shown by the square points at $\sim 0.01R/R_{200}$) however, do show a trend for increasing time since quenching as the number of group galaxies increases (Figure 5.10a), but the rate at which they quench is the same (Figure 5.10d) suggesting the mechanism by which this occurs is the same for all centrals regardless of halo mass.

In the top panels of Figure 5.11 the GZ2-GROUP satellite galaxies are split into bins of their relative velocity to their central galaxies, i.e. the velocity at which they move through the dense group environment. There is no trend with either time since onset of quenching (Figure 5.11a) or rate of quenching (Figure 5.11b) with increasing relative velocity for galaxies in the GZ2-GROUP sample. This suggests that whatever quenching mechanism is occurring in groups, it is not correlated with the velocity at which satellites move through the dense environment.

The bottom panels of Figure 5.11 show the trend with group radius for the GZ2-GROUP satellites when split into bins of galaxy stellar velocity dispersion σ_* (note that this is not the velocity dispersion of the group) which is often used as a proxy for the galaxy potential. The stellar velocity dispersion show the largest trend in Δt (Figure 5.11c) for satellite galaxies of all of the group or satellite galaxy properties studied, with galaxies with the smallest stellar velocity dispersions having quenched more recently. Although this trend is less apparent in Figure 5.11d for the rate that quenching occurs with σ_*, it is the largest trend see across the right panels of Figures 5.9-5.11. Also, field galaxies (shown by the circles at $\sim 25R/R_{200}$) with low velocity dispersions are seen to quench at much slower rates than their satellite counterparts. This suggests that the rapid quenching observed for the low stellar velocity dispersion satellites is directly caused by the environment.

5.3 Discussion

5.3.1 The role of mergers as quenching mechanisms in the group environment

The merger classification in GZ2 has been shown to preferentially identify major mergers (Darg et al., 2010b); whereas, bulge formation in disc galaxies is often associated with minor merger driven evolutionary histories (Croton et al., 2006; Tonini et al., 2016). Although we see evidence for an enhanced merger fraction in the inner regions of the group environment in Figure 5.7, the bulge fractions in Figure 5.8 vary much more significantly from the field value than the merger fraction. This suggests that minor mergers may be more dominant than major mergers for satellites in the group environment, particularly at $R/R_{200} > 0.5$.

If mergers are a dominant evolutionary mechanism for satellite galaxies, as the morphological evidence in Figures 5.7 & 5.8 suggests, we would expect to see a difference in the quenching histories of satellites residing in groups with a larger number of members. However, the top panels of Figure 5.10 show there is no trend with time since quenching onset or rate of quenching with increasing N_{group} for the satellite galaxies. This suggests that mergers are not the dominant quenching mechanism for satellite galaxies, but that whatever mechanism is the cause of the quenching occurs at the same rate irrespective of group size.

Central galaxies however, do show a trend for increasing time since quenching with increasing N_{group} (square points at $0.01R/R_{200}$ in Figure 5.10a) occurring at a rate of $\tau \sim 1$Gyr, which as discussed in Chapter 3, was attributed to mergers and galaxy interactions which could transform a galaxy's morphology. Therefore, the larger the number of group members, the more important mergers are for a central's evolutionary history. This is in agreement with the findings of Lin et al. (2010); Ellison et al. (2010); Lidman et al. (2013) and also McIntosh et al. (2008) who found in a sample of local groups and clusters that half of the mergers they identified involved the central galaxy. Liu et al. (2009) also found that the fraction of merging centrals increases with the richness of a cluster (a measure of the number of galaxies within $1h^{-1}$Mpc of the central galaxy).

This idea is supported by the result in Figure 5.9a showing that centrals of a given mass have quenched more recently than the inner satellites (at $\sim 0.1R/R_{200}$) of a given mass. This suggests that an episode of more recent star formation, such as a starburst, may have occurred in the central galaxies but not in the inner satellites. Mergers are thought to cause an energetic burst of star formation which can in turn quench the remnant galaxy (Hopkins et al., 2005; Treister et al., 2012; Pontzen et al., 2016, as discussed in Section 3.3.1). This result is once again suggestive of a merger dominated history for central galaxies but not for satellite galaxies.

5.3.2 The role of mass quenching in the group environment

A trend is seen for increasing time since quenching with increasing stellar mass and velocity dispersion (a proxy or galaxy potential) for centrals, satellites and field galaxies in Figure 5.9a and Figure 5.11c respectively. This is suggestive of mass quenching occurring across the entire galaxy population irrespective of environmental density, supporting the work of Peng et al. (2010, 2012); Gabor et al. (2010) and Darvish et al. (2016).

5.3.3 The role of morphological quenching in the group environment

The increasing bar fraction toward the central group regions shown in Figure 5.6 (in agreement with Skibba et al., 2012), suggests that bars may be partly responsible for the relation between quenched fraction and environmental density. This is consistent with findings that show that bars themselves may be the cause of morphological quenching through the funnelling of gas toward the central regions of galaxies (Athanassoula, 1992b; Sheth et al., 2005; Masters et al., 2010a) which is then used in star formation, exhausting the available gas. As discussed in Chapter 4, an inflow due to a bar may also be able to fuel an AGN. The AGN-environmental connection has been extensively studied[1] with conflicting results; Pimbblet et al. (2013), with optically selected AGN, and Ehlert et al. (2014), with X-ray selected AGN, showed that the AGN fraction decreases towards the inner regions of groups. However, these studies did not take into account the morphology-density relation of satellite galaxies, where bugle dominated galaxies dominate in the inner regions of groups. Miller et al. (2003) and more recently de Souza et al. (2016), using a hierarchical Bayesian method, showed with optically selected AGN that although the AGN fraction decreases with group radius for early-type galaxies, it stays constant with group radius for late-types. This suggests that disc galaxies are still able to fuel their AGN even in dense environments, perhaps due to the enhanced bar fraction in the inner regions of the group.

We must therefore consider whether the environment itself may play a role in triggering the disk instabilities which can produce a bar. Indeed harassment and tidal interactions, believed to be common in the group environment, have been shown to both promote and inhibit bar formation dependent on the stellar mass (Noguchi, 1988; Moore et al., 1996; Skibba et al., 2012). If the environment was indeed triggering a bar, then morphological quenching would be occurring in the group environment but indirectly due to environmental quenching. This suggests that the polarity between internal secular processes ('nature') and external environmental processes ('nurture'; proposed by Peng et al. 2010) may not be as extreme as first thought, in agreement with Skibba et al. (2012).

5.3.4 The role of the environment in quenching

Across all panels of Figures 5.9-5.11 a trend for increasing time since quenching onset with decreasing group radius is present. I interpret this as the environment directly causing quenching at the same rate throughout the infall time of a galaxy in a group. Those galaxies closer in, fell into the group earlier and as they did so they started to quench, giving rise to a larger inferred Δt.

[1] I attempted to study this in this investigation however only 204 satellites and 128 centrals of the GZ2-GROUP sample were identified as obscured Type 2 AGN using a BPT diagram. These low numbers of AGN mean that when split into bins of group radius we are well and truly dancing precariously on the low number statistics volcano and so no robust conclusions can be drawn.

More massive halos are seen to have a greater impact on the star formation histories of their satellites than less massive halos in Figure 5.9c. The halo mass is correlated with both (i) the gravitational potential of the group and (ii) the temperature of the IGM, suggesting that an environmental quenching mechanism which is correlated with one of these properties is responsible for this result.

Higher mass halos have hotter intra group medium (IGM) temperatures (Shimizu et al., 2003; Del Popolo et al., 2005) which can have a greater impact impact on a galaxy through ram pressure stripping (RPS) of cold gas. Gunn & Gott (1972) define the ram pressure as:

$$\rho_{\mathrm{IGM}} \cdot v^2 = 2\pi G \cdot \sigma_*(R) \cdot \sigma_g(R), \tag{5.4}$$

where ρ_{ICM} is the density of the IGM, $\sigma_*(R)$ the star surface density, $\sigma_g(R)$ the gas surface density of the galaxy disc and v the velocity of the galaxy through the IGM. Therefore if RPS is indeed a dominant environmental quenching mechanism we should see a trend in Δt with the velocity of a satellite relative to its central galaxy. However in Figure 5.11a we see that this is not the case. This therefore rules out RPS as the dominant environmental quenching mechanism, in support of the conclusions of simulations by Emerick et al. (2016); Fillingham et al. (2016) and observations by McGee et al. (2014). However, this conclusion may be due to the stellar mass range spanned by the GZ2-GROUP satellite galaxies which all have $M_* \geq 10^9 \mathrm{M}_\odot$, as simulations by Fillingham et al. (2016) suggest that RPS only becomes effective in lower mass satellites with $M_* \leq 10^{8-9} \mathrm{M}_\odot$, in agreement with Hester (2006).

Above this mass threshold in the simulations of Fillingham et al. (2016), a 'starvation' mode (Larson et al., 1980; Balogh et al., 2000) dominantes, where a galaxy's extended gaseous halo is removed causing a quench, as cold gas for use in star formation can no longer be fed from the extended halo. Such a mechanism will be correlated with the galaxy potential, as galaxies with a lower potential will be most easily stripped of their halos. This is apparent in Figure 5.11d where satellites with lower velocity dispersion (a proxy for the galaxy potential) are more rapidly quenched than their higher velocity dispersion counterparts and those in the field. Such a starvation mechanism is also correlated with the group potential, which is correlated with the halo mass, for which similar trends in Δt are see in Figure 5.9c. The dominant environmental quenching mechanism occurring in the group environment must therefore be correlated with the group potential. This suggests that satellite galaxies may be most affected by gravitationally driven environmental effects, such as starvation, thermal evaporation of the galaxy halo and galaxy harassment.

If we assume that galaxies begin their infall into a group at a radius of $\sim 10\mathrm{R}_{200}$ we can calculate the infall time of the satellites from the difference in Δt to a radius of $0.1\mathrm{R}_{200}$, $\delta\Delta t = \Delta t_{0.1R_{200}} - \Delta t_{10R_{200}}$. In Figure 5.10a the trend seen in Δt with group radius is the same regardless of the number of galaxies in the group, so we can estimate an average infall time of $\delta\Delta t \sim 3$ Gyr for the GZ2-GROUP satellites. The rate of quenching occurring across the group radius in Figure 5.10b is $\tau \sim 1$ Gyr and so we can also estimate the average quenching timescale (i.e. the time taken to fully quench from the SFS to 5σ below the SFS, as in Chapters 3 & 4) to be ~ 4 Gyr for the GZ2-GROUP satellites.

This infall time and quenching timescale are in agreement with the estimates of Wetzel et al. (2013) who used a high resolution cosmological N-body simulation to track satellite galaxy orbits in SDSS groups and clusters and found quenching timescales of $2-6$ Gyr. Using a similar method, Oman & Hudson (2016) derive an infall time of ~ 4 Gyr and quenching timescales between $4-6$ Gyr for galaxies in the mass range of the GZ2-GROUP sample. Similarly, Hahn et al. (2016) derive a total quenching timescale of ~ 4 Gyr for satellite galaxies on infall into the group environment. However, the simulations by Fillingham et al. (2016) and Emerick et al. (2016) have shown that RPS cannot remove enough gas mass to completely quench the galaxy within ~ 2 Gyr but can assist in reducing the starvation timescale so that galaxies can be quenched within the ~ 4 Gyr quenching timescale calculated in this study. This suggests that although the effects of mechanisms correlating with the group potential are detectable in the quenching parameters of the GZ2-GROUP sample, this is only made possible by the constantly present, but less dominant effects of ram pressure stripping.

This conclusion, along with the discussion in Section 5.3.3 that morphological quenching may only be present in the group environment due to the influence of the environment itself, suggests that all mechanisms discussed here will affect a galaxy, at some point in its lifetime, which is infalling through the group environment. A single mechanism may be more dominant in the evolution of an individual galaxy but to achieve the correlations between morphology, colour and quenched galaxy fraction with density observed across the entire population all mechanisms need to act in concert.

5.4 Conclusions

Using the Berlind et al. (2006) group catalog, I have constructed a sample of group galaxies in the SDSS which were cross matched with Galaxy Zoo 2 and GALEX in order to determine their most likely SFHs using STARPY. I have shown that although mass quenching, morphological quenching and mergers are all important mechanisms at work in quenching the galaxies in the group environment, the environment does play a role in quenching galaxies as they infall into the group. I have discussed the possibility that not one mechanism will dominate across the group population, with all mechanisms acting collaboratively. My findings are summarised as follows:

(i) The bar, obvious bulge and merger fractions are all seen to increase above the field value in the inner regions of the groups of the GZ2-GROUP sample in Figures 5.6, 5.8 & 5.7 respectively.

(ii) Mergers are the dominant quenching mechanism for central galaxies but not for satellite galaxies. Satellites may undergo a minor merger in the group environment but there effects are only discernible by their indirect effect on the bulge fraction (see Figure 5.8).

(iii) Mass quenching is occurring across the entire GZ2-GROUP sample for centrals and satellites irrespective of the environmental density (see Figure 5.9a).

(iv) Morphological quenching is occurring for GZ2-GROUP satellite galaxies as evidenced by the heightened bar fraction in the inner group regions (see Figure 5.6). However, this may be indirectly due to environmental quenching since galaxy interactions and harassment are believed to be able to trigger bars. This suggests the polarity between 'nature' vs. 'nurture' may not be as extreme as previously thought.

(v) The environment does cause quenching across the GZ2-GROUP sample, as evidenced by the increase in the time since quenching with decreasing group radius seen across all left panels of Figures 5.9-5.11. The results in Figures 5.9a & 5.11c suggest that this is caused by a quenching mechanism correlated with the group potential, such as harassment, interactions and starvation, rather than the velocity of a satellite through the group, such as ram pressure stripping. This quenching occurs within an average quenching timescale of ~ 4 Gyr from star forming to complete quiescence, after an average infall time of ~ 3 Gyr.

It is apparent from the results presented in this Chapter that many quenching mechanisms are all occurring simultaneously in the group environment; therefore a superposition of all of the effects of these mechanisms is seen in the quenching histories of the GZ2-GROUP sample, which in turn gives rise to the morphology-density relation observed.